Title no. 102-S81

CCT Nodes Anchored by Headed Bars— Part 1: Behavior of Nodes

by M. Keith Thompson, Michele J. Ziehl, James O. Jirsa, and John E. Breen

The anchorage behavior of headed reinforcement in compression-compression-tension (CCT) nodes was studied experimentally. Observations of cracking behavior and measurements of strains in ties and confining reinforcement, head slip, and node and strut capacities are reported. The behavior of unconfined nodes is compared with confined nodes. Insight into the stress state of the node is obtained through strain measurements along ties and along confining steel around the node. The strain data show node failure to be related primarily to anchorage of the tie bar. Additionally, the anchorage of headed reinforcement is explored. Headed reinforcement anchorage is shown to consist of bond and head-bearing components. These components develop in separate stages such that bond generally peaks and begins to decline before head bearing peaks. The two components do not achieve peak capacity simultaneously.

Keywords: anchorage; reinforcement; strut; ties.

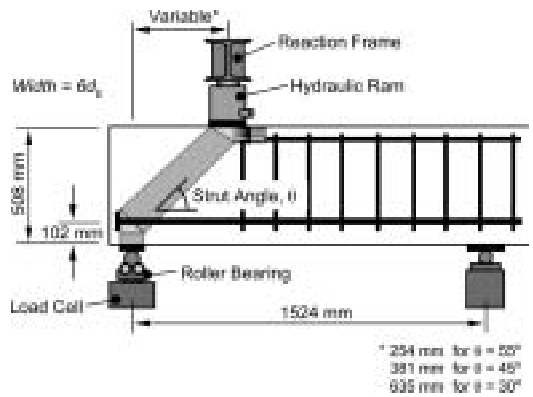

Fig. 1—Unconfined CCT node test specimen.

INTRODUCTION

The Texas Department of Transportation (TxDOT) funded a program to study the feasibility of using headed reinforcement in bridge structures. After considerable examination of a variety of potential applications, it was decided that headed reinforcement provided a promising solution for many complex discontinuity regions in which the constraints of geometry provide very little space for anchorage of reinforcement. Such discontinuity regions include the ends of bridge bents, anchorage diaphragms, and deviator blocks in post-tensioned bridges. TxDOT has conventionally used hooked bars in such situations, but hooks can sometimes lead to congestion of the reinforcing cage and make casting difficult. Because compression-compression-tension (CCT) nodes are a common element within these discontinuity regions, a program of study focusing on the behavior of headed reinforcing bars in CCT nodes was developed. In a companion study, the behavior of lap splices with headed bars was examined. This report is Part 1 of a two-part article that deals solely with the results of the CCT node study. In Part 1, data relevant to the mechanics of CCT nodes and to anchorage of headed reinforcement is presented. In Part 2, the capacity of nodes is discussed and several models for determining the capacity of CCT nodes and headed reinforcement are compared.

Few previous studies have provided experimental data on CCT nodes or of the anchorage behavior of headed reinforcement in CCT nodes. An experimental study of CCT nodes was conducted by Barton et al.[1] who tested 10 isolated CCT specimens anchored by multiple layers of straight 16 mm bars. The majority of these specimens failed by anchorage loss of the tie reinforcement. Armstrong et al.[2] and Wood, Kreger, and Breen[3] studied bridge pier overhangs with headed bars as the primary tie reinforcement. The end support represents a typical CCT node situation. Aguilar et al.[4] reported on four tests of deep beams. In two of these beams, the primary tension reinforcement was anchored by heads in CCT nodes at the end supports of the beams. In the latter two studies, the head sizes were large enough to prevent anchorage failure at the node before yielding of the tie bars. The cumulative data from these three studies has demonstrated the difficulty of providing sufficient development length for straight bars in CCT nodes and the potential of headed reinforcement for solving this problem. Neither of these studies, however, has thoroughly explored the conditions for anchorage failure of headed reinforcing bars. Specific data are lacking in regards to the mechanisms of anchorage failure and the general trends in anchorage capacity with respect to many significant variables, primarily with respect to head size, concrete cover, concrete strength, strut angle, and anchorage length. Without such data, guidelines for the detailing of headed reinforcement at nodes cannot be produced.

RESEARCH SIGNIFICANCE

Sixty-four CCT node specimens were tested. The results of these tests provide important experimental information on the behavior and failure modes of CCT nodes. Furthermore, the test results provide information on the anchorage behavior of headed reinforcement. The observations of these tests provide a basis for developing realistic models of headed reinforcement anchorage.

TEST PROGRAM

A typical unconfined specimen is shown in Fig. 1. The critical CCT node is at the bottom left of the specimen,

ACI Structural Journal, V. 102, No. 6, November-December 2005.
MS No. 03-464 received October 16, 2003, and reviewed under Institute publication policies. Pertinent discussion including author's closure, if any, will be published in the September-October 2006 *ACI Structural Journal* if the discussion is received by May 1, 2006.

ACI member **M. Keith Thompson** *is an assistant professor at the University of Wisconsin-Platteville, Platteville, Wis. He received his BS from North Carolina State University, Raleigh, N.C., and his MS and PhD from The University of Texas at Austin, Austin, Tex. His research interests include anchorage of reinforcement and strut-and-tie modeling.*

Michele J. Ziehl *is a PhD student in civil engineering at Tulane University, New Orleans, La. She received her BS from Marquette University, Milwaukee, Wis., and her MS from The University of Texas at Austin. Her research interests include the behavior of structural concrete and fiber-reinforced polymers.*

James O. Jirsa, *FACI, holds the Janet S. Cockrell Centennial Chair in Engineering at the University of Texas at Austin. He is a Past President of ACI, a member of the ACI Board of Direction, and a Past Chair of the Technical Activities Committee. He is a member of ACI Committees 318, Structural Concrete Building Code; 408, Bond and Development of Reinforcement; and is a member and Chair of Subcommittee 318-F, New Materials, Products, and Ideas.*

ACI Honorary Member **John E. Breen** *holds the Nasser I. Al-Rashid Chair in Civil Engineering at the University of Texas at Austin. He is a member and Past Chair of ACI Committee 318, Structural Concrete Building Code; is a member of ACI Committees 318-B, Reinforcement and Development; 318-E, Shear and Torsion; 355, Anchorage to Concrete; and is a Past Chair of the Technical Activities Committee.*

created by the intersection of the vertical strut from the bottom bearing support, the diagonal compression strut from the point of load application, and the horizontal (tension) tie bar. A detail of this node is provided in Fig. 2. The tie bar was either a single 25 or 36 mm bar. The width of the specimen was typically six tie bar diameters ($6d_b$). The bottom bearing plate was rigid and always full width, with a typical length of $4d_b$. The angle of the diagonal compression strut (θ_{strut}) was varied by changing the point of load application. Specimens were tested with 30-, 45-, and 55-degree strut angles. Typically, no secondary steel was placed near the node or along the length of the strut. However, some confined specimens with stirrups or special details in the node region were tested. The details of the stirrup-confined node specimens are shown in Fig. 3. Various head sizes and shapes were used to anchor the tie bar. Head size was characterized by the relative head area, defined as the ratio of net head-bearing area (A_{nh}) to the cross-sectional area of the bar (A_b). The net head area excludes the bar area. Head size varied from nonheaded (relative head area, A_{nh}/A_b = 0.0) to large (A_{nh}/A_b = 10.4 maximum). Circular, square, and rectangular shaped heads were tested. Rectangular shaped heads were tested with two possible orientations: vertical (in which the longer dimension was placed parallel to the plane of the strut-and-tie model) and horizontal (in which the longer dimension was placed perpendicular to the plane of the strut-and-tie model). Some specimens with hooked tie bars were also tested. Concrete strength f_c' was 21 to 28 MPa. The concrete strength was deliberately kept low to produce failure of the node before yielding of the tie bar could occur. Details of all tests are included in Part 2 of this paper.

Slip at the head of the tie bar, the bearing reaction under the node, deflection at the load point, and strains along the tie bar (via strain gauges) were measured. The typical locations of strain gauges on the tie bar are shown in Fig. 2. In some specimens, additional strain gauges were placed on the tie bar or on confining stirrups or special reinforcement details within the diagonal strut and node zone. Load was applied monotonically via a hydraulic ram activated by a hand pump. Specimens were loaded in 5 to 10 kN increments until the specimen was perceived to be near failure and then in 2 to 4 kN increments until failure occurred. The total time of testing was approximately 45 minutes including several 5-minute pauses in the loading to mark cracks and take photos.

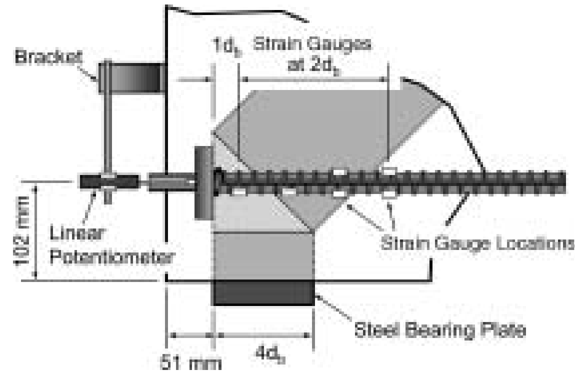

Fig. 2—Detail of unconfined CCT node.

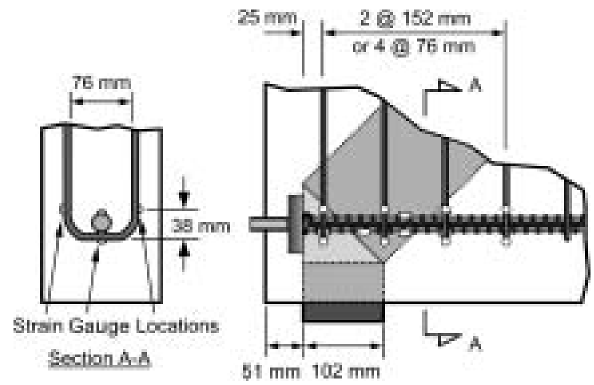

Fig. 3—Details of confined CCT node specimens.

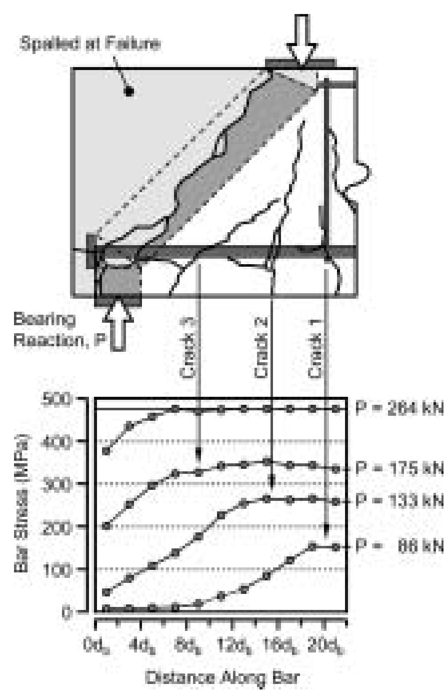

Fig. 4—Development of tie bar at various load stages.

TEST RESULTS

Unconfined CCT nodes

The mechanics of stress transfer in the node—The crack pattern for a CCT node specimen with a 25 mm-diameter tie bar with a 76 x 76 mm head (relative head area = 10.4), strut angle of 45 degrees, and f_c' of 28 MPa is shown in Fig. 4, and is typical of the node tests. First cracking occurred at the

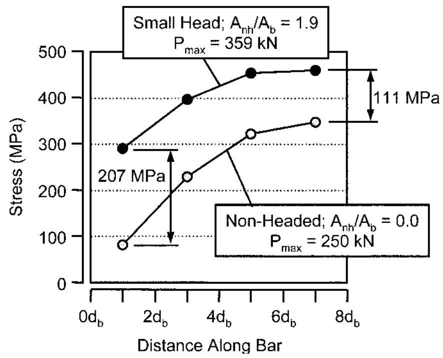

Fig. 5—Development of headed and nonheaded tie bars.

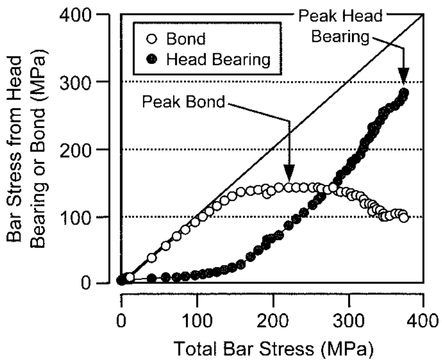

Fig. 6—Bond and head bearing components of tie anchorage.

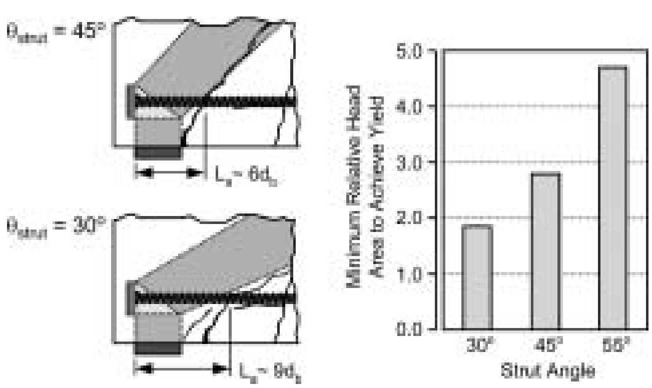

Fig. 7—Effect of strut angle on anchorage of tie bar.

point of maximum moment (directly beneath the load point). The measured front bearing reaction P was 64 kN. Subsequent cracks formed at regular intervals toward the nodal zone (Crack 2 at P = 116 kN and Crack 3 at P = 141 kN) until the truss mechanism was fully developed. Horizontal bond splitting cracks formed between adjacent diagonal cracks. Failure, marked by explosive rupture at the node and spalling of the end of the beam (the triangular concrete section shown in Fig. 4 above the diagonal strut), occurred at P = 265 kN.

Twenty-two strain gauges were placed along the top and bottom of the reinforcing bar to measure the stress profile along the tie. (This particular specimen had more strain gauge instrumentation than was typical. Each data point in Fig. 4 is the average of gauge measurements from the top and bottom of the tie bar.) Stress profiles from each stage of cracking demonstrate the evolution of tie anchorage. With the formation of each successive crack approaching the nodal zone, the anchorage length of the tie bar shortened. Eventually, development of maximum bar stress occurred at a distance of about $7d_b$ from the bearing face of the head. There was little change in the shape of the stress profile following the formation of Crack 3 at about 53% of the maximum load. The final point of maximum bar stress could be conservatively estimated as the point where the tie bar leaves the path of the diagonal compression strut (this region is referred to as the “extended nodal zone” in the provisions of ACI 318 Appendix A).[5] The final stress profile, just prior to failure of the specimen, shows that the head carried about 377 MPa and that an additional 95 MPa was provided by bond along the bar between the strain gauge closest to the head and the point of maximum bar stress (about $6d_b$). At failure, about 80% of anchorage was provided by head bearing and about 20% by bond.

Stress profiles from CCT node tests with headed and nonheaded tie bars are shown in Fig. 5. Both specimens shared the following details: the strut angle was 55 degrees, the concrete strength f_c' was 27 MPa, and the diameter of the tie bar was 25 mm. The headed bar specimen had a 38 x 38 mm head (relative head area equals 1.9). The CCT node with the nonheaded tie bar reached a maximum bearing reaction of 250 kN before failure. The stress profile indicated a maximum bar stress of 346 MPa at a distance of seven bar diameters (175 mm) from the end of the bar. The rate of change of the bar stress within the anchorage length was very rapid. Extrapolation of the curve indicated a stress of zero at the end of the bar. Inclusion of a small head significantly improved the capacity of the node to 359 kN (a 44% increase over the nonheaded case). The stress at the end of the tie bar increased by 207 MPa. The bar stress in the headed bar, however, was only 111 MPa greater at a distance of $7d_b$ from the bar end. The difference in bar stress between the head and the critical stress point (at approximately $7d_b$) was provided by bond along the bar. If the bond along the two tie bars was the same, then the offset between the two profiles would be constant. The offset, however, decreased along the bar length, indicating that bond along the headed bar was less than that of the nonheaded bar. Similar behavior was observed in all of the CCT node tests, with bond at failure decreasing as larger heads were added to the tie bar.

Using the stress profile data, the components of bar anchorage provided by bond and head bearing could be differentiated and tracked. Typical data for these components are plotted in Fig. 6. The data were measured in a specimen with a 36 mm-diameter tie bar with a 51 x 76 mm head (relative head area equal to 2.85, head oriented vertically), strut angle of 45 degrees, and f_c' of 28 MPa. The bond contribution was determined from gauges placed at $7d_b$ from the face of the head. The early rise in the bond component shows that the bar force was initially transferred to the concrete primarily by bond. As the bar force increased, however, the bond component leveled off, and further increases in bar stress were transferred by head bearing. Eventually the bond contribution declined while the head bearing component rose rapidly. Peak bond stress did not occur simultaneously with peak head bearing. At failure, the anchorage capacity of the headed bar was provided by peak head bearing plus reduced bond. Larger heads increased head bearing but resulted in larger decreases in the bond component. Thus, larger head sizes were generally associated with smaller bond at failure.

Effect of strut angle—The effect of decreasing strut angle is shown in Fig. 7. Decreases in strut angle caused the strut path to include more of the tie bar, thus increasing the length

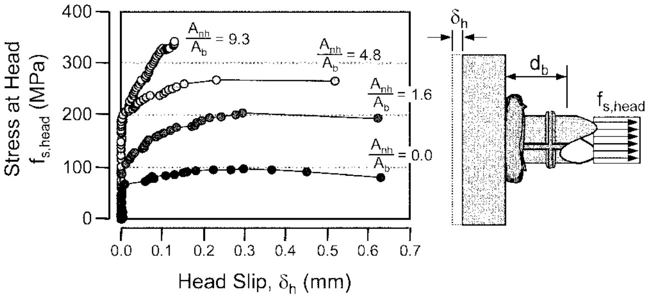

Fig. 8—Bar stress at head versus head slip.

of the extended nodal zone (schematically shown by the drawings on the left in Fig. 7). Increases in the length of the extended nodal zone increased the distance between the head and the point of maximum bar stress, providing a greater length for bond to act on the tie bar. Increases in the bonded length of the tie bar increased the overall contribution from bond to tie anchorage. As the bond contribution increased, a smaller head bearing contribution was necessary to attain yield stress. Thus, as the strut angle decreased, smaller head sizes were required to generate yielding. This trend is shown by the test data plotted on the right in Fig. 7.

Head slip—Head slip is plotted against the bar stress at the head in Fig. 8. The bar stress at the head was determined from a strain gauge placed one bar diameter from the head face. Data are presented for four specimens with 36 mm-diameter tie bars. Data for four different head sizes are shown: no head, 51 x 51 mm, 76 x 76 mm, and 102 x 102 mm (relative head areas are given in the figure). All specimens had 45-degree strut angles and concrete strength f_c' between 27 to 28 MPa. Head slip typically did not initiate until anchorage failure was imminent, and then increased rapidly up to the point of failure. Initiation of slip was delayed as head size increased. For the nonheaded bar (relative head area equals 0.0), slip increased rapidly at low stress levels. The addition of a small head (relative head area equals 1.6) doubled the peak bar stress at a head slip of 0.3 mm. An increase in relative head area from 1.6 to 4.8, however, increased the bar stress at the head by only about 35% (from 200 to 270 MPa). Increases in head size provided higher capacity and less slip; however, the rate of increase of stress at first slip and at ultimate diminished with larger increases in head area.

Failure modes—CCT node specimens failed in one of three different modes: 1) pullout of the tie bar from the node region (this mode occurred only for nonheaded, straight bars); 2) rupture of the node region; or 3) yielding of the tie bar. Figure 9 shows photos of the nonductile failure modes. Unless yielding of the tie bar occurred, failure was sudden and brittle.

Pullout failure of the tie bar in Fig. 9(a) was indicated by pronounced widening of the primary diagonal crack at the edge of the extended nodal zone and horizontal bond splitting cracks propagating into the CCT node.

Rupture with lateral splitting along the path of the diagonal strut is shown in Fig. 9(b) for a bar with relative head area of 2.8. The strut was cleaved into two distinct pieces along its length. Between the head and the bottom bearing plate, a pyramid-shaped zone of concrete was crushed, leaving the void shown below the head in the close-up view on the right.

Rupture with crushing of the concrete is shown in Fig. 9(c), along the portion of the strut just above the head (relative head area equals 4.13). The width of the crushed zone was

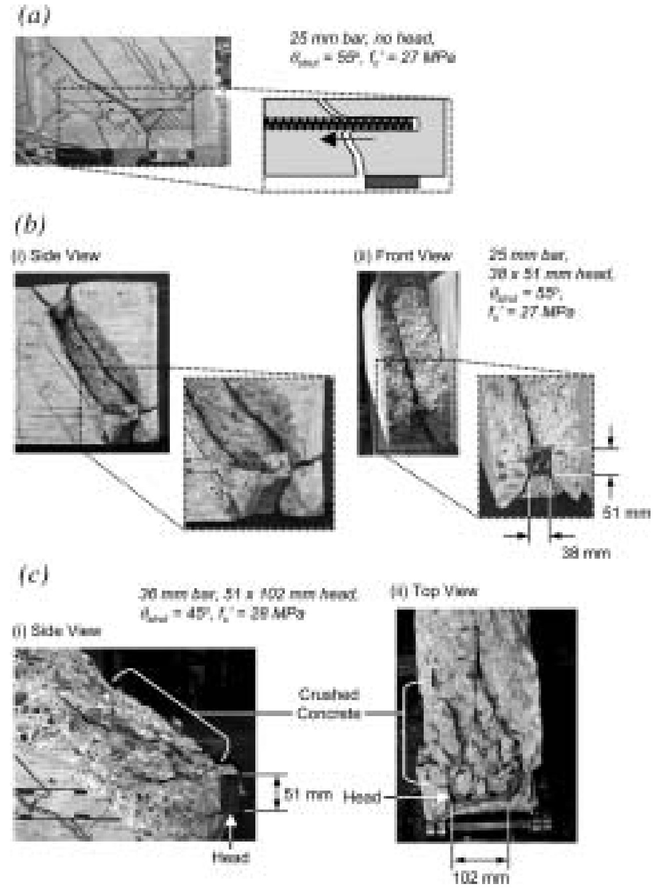

Fig. 9—Photos of node failures: (a) nonheaded bar pullout failure; (b) headed bar failure with lateral splitting; and (c) headed bar failure with crushing of concrete.

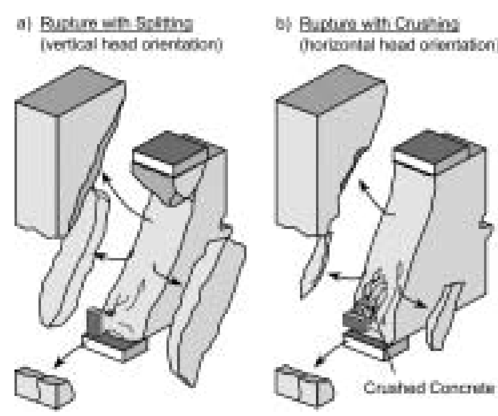

Fig. 10—Rupture of nodal zone (rectangular heads).

slightly greater than the width of the head. The length of the crushed zone along the strut was about 2.5 times the width of the head. Outside of the zone of crushing, some lateral splitting of the strut was observed, but not as distinctly as the specimen shown in Fig. 9(b).

Rupture failures provided the most information regarding node behavior. Rupture of the node typically exhibited two characteristics: 1) lateral splitting initiating in the nodal region that propagated up the diagonal compression strut; and 2) crushing of the concrete between the head and the diagonal strut path. The degree to which these two characteristics were present in a rupture failure was dependent on the size and orientation of the head as shown in Fig. 10. Smaller,

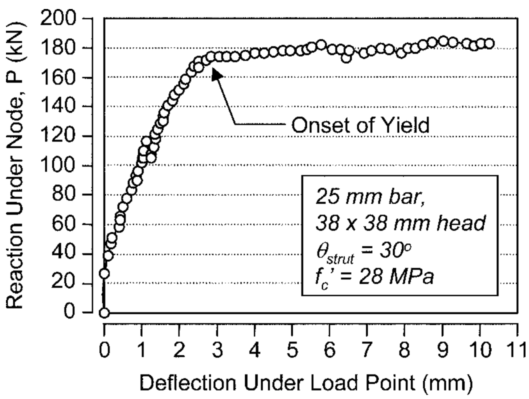

Fig. 11—Load-deflection curve indicating ductile failure.

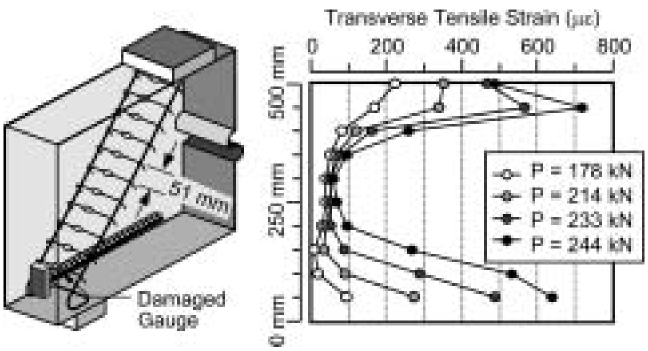

Fig. 12—Profiles of lateral splitting strain.

vertically oriented heads (that is, for rectangular heads oriented so that the long axis of the head was perpendicular to the bottom bearing plate) tended to cleave the concrete transversely and created more lateral splitting at failure. Larger, horizontally oriented heads tended to cause more crushing of the concrete, though some transverse splitting usually occurred.

Yielding of the tie bar was achieved with large heads. A ductile failure is shown in Fig. 11. It is important to note that ductility was achieved even though the node was unconfined and the strut contained no supplementary reinforcement. All that was necessary for ductility was the provision of sufficient tie bar anchorage (head bearing plus bond length).

Confined CCT nodes

A limited number of tests of confined CCT node specimens and specimens with special reinforcement details provided means for measuring strains in the nodal zone. These results were useful for understanding the failure modes of the specimens.

Transverse splitting strains—To better understand the initiation of lateral splitting during node rupture, one specimen was specially instrumented with 11 strain gauges spaced at 51 mm along the length of the diagonal compression strut and oriented in the direction of the splitting stress (Fig. 12). This specimen contained a 25 mm-diameter bar anchored by a 38 x 76 mm head (relative head area equals 4.7). The head was oriented with the long axis vertical to deliberately precipitate lateral splitting of the node and strut. The strut angle was 45 degrees. The strain gauges were attached to 4.8 mm plain steel wire. The concrete strength was 28 MPa.

Data from this test are presented on the right in Fig. 12. The transverse strain profile of the diagonal compression

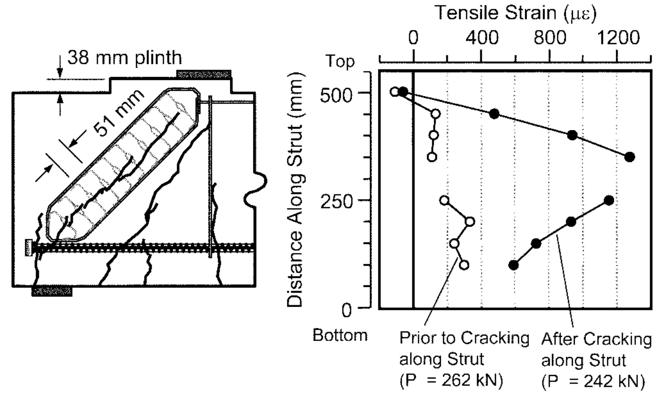

Fig. 13—Profiles of in-plane splitting strain.

strut is shown for four different load stages. The shape of the profiles indicates that transverse splitting initiates at the ends of the strut (much like a double punch tensile test). Little transverse tension ever developed in the middle of the strut. The maximum tensile strain was approximately equal at the top and bottom of the strut. The lower strain at the top strain gauge was likely due to platen restraint from the load plate. Based on these results, the transverse splitting can be characterized as the cleaving of the strut laterally by wedges that formed at one or both ends of the strut.

In-plane splitting—In another specimen, 10 strain gauges were placed along the length of the strut to measure splitting strains in the plane of the specimen (Fig. 13). This specimen was similar to the previous one, except that the head was oriented horizontally. Also, a small plinth was placed on the top surface of the specimen to provide space for the bars to which the strain gauges were attached. The concrete strength was 26 MPa.

Data from this test are presented on the right in Fig. 13. In-plane strain profiles are presented for two load stages: 1) just prior to cracking along the diagonal strut; and 2) after cracking along the strut. Data are missing from the middle and lower portion of the plot due to damaged strain gauges. There was little in-plane tension prior to strut cracking. Before cracking, the greatest tension in the strut was near the head of the tie bar. Just prior to cracking, the measured strains in the nodal region were approximately 300 με. The specimen cracked along the strut as the next increment of load was applied. Capacity immediately dropped. The strain evidence suggests that the strut cracking was initiated by the tensile stress created at the head of the tie bar.

Following strut cracking, the drop in capacity was not recovered. The specimen continued to lose strength as deformation of the beam increased. With the initiation of strut cracking, tension within the strut shifted to the middle. This tension was carried entirely by the instrumentation detail, which acted as reinforcement for the strut. This detail was constructed from 4.8 mm-diameter plain steel wire. With more substantial strut reinforcement, the specimen may have sustained its precracking peak capacity through larger deformations. The specimen eventually failed by rupture of the CCT node and transverse splitting along the strut.

Specimens confined by stirrups—Five specimens were tested with stirrups to confine the nodal zone. Stirrups were used because they represented a common form of reinforcement that may be expected at a nodal zone. Two specimens had nonheaded bars, two had headed bars (38 x 76 mm with the head oriented vertically) (refer to Fig. 3), and one had a

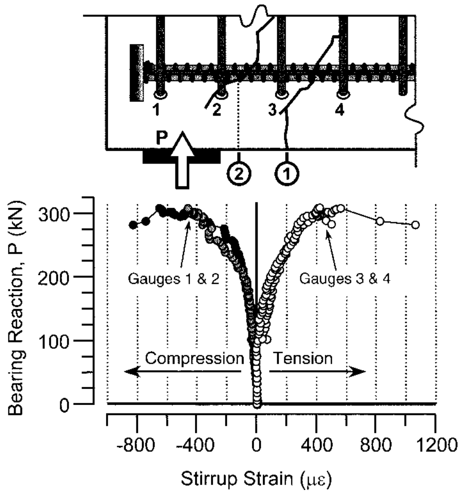

Fig. 14—Lateral stirrup strain in confined CCT node.

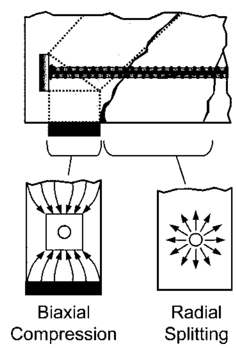

Fig. 15—Zones of compression and tension at CCT node.

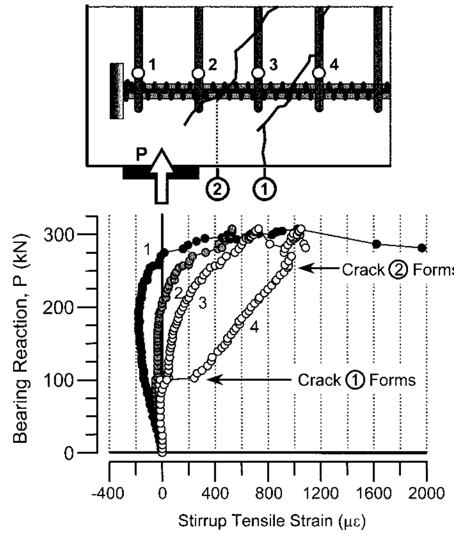

Fig. 16—Vertical stirrup strain in confined CCT node.

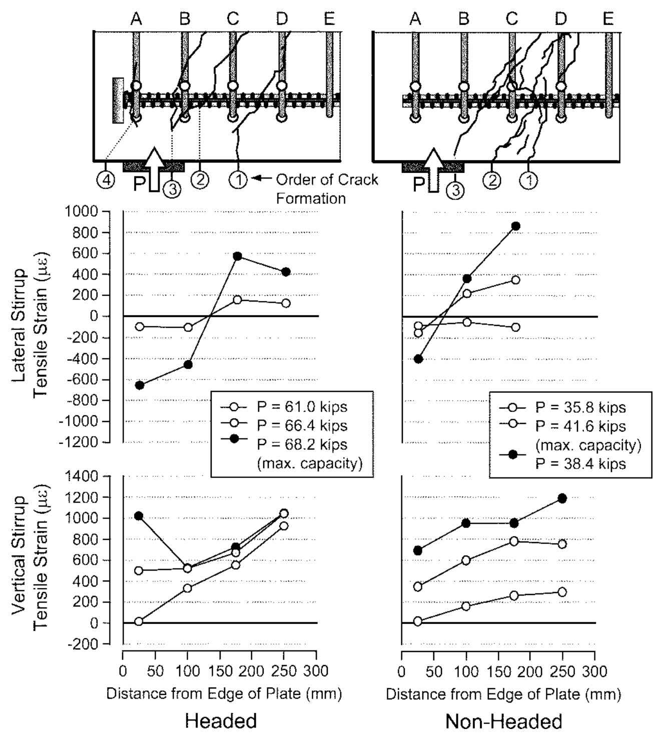

Fig. 17—Vertical stirrup strain in confined CCT node.

standard hook. All tie bars were 25 mm in diameter. The stirrups were 10 mm-diameter bars bent in closed hoops, spaced at 76 or 152 mm within the CCT node region (providing ratios of strut reinforcement, $[A_{sv}/bs] \cdot \sin[45 \text{ degrees}]$, equal to 0.0086 and 0.0043, respectively). Additionally, all stirrup-confined specimens had 45-degree strut angles and concrete strength equal to 26 MPa. Strain gauges placed on the stirrup bars provided useful information about the stress state of the concrete in that region of the specimen.

Gauges placed on the bottom of the stirrups measured lateral strains along the underside of the tie bar. These strains are plotted in Fig. 14. The data show two distinct zones of lateral strain. Within the extended nodal zone, the tie bar was placed under increasing lateral compression as load was placed on the specimen (as shown by Gauges 1 and 2 in Fig. 14). The bearing stress uniformly applied across the width of the specimen at the reaction bearing plate must neck inward toward the smaller width of the tie bar. The redirection of this compression stress produces lateral compression (refer to Fig. 15). Combined with the vertical compression caused by the compression struts, a state of biaxial compression is created. Outside of the extended nodal zone, radial splitting caused by bond along the tie bar produced increasing lateral tension as load was placed on the specimen (as shown by Gauges 3 and 4 in Fig. 14). Figure 15 schematically illustrates the differences between the two regions.

Gauges placed on the sides of the stirrups measured vertical strain along the tie bar. These strains are plotted in Fig. 16. Each data point is the average of two gauges placed on both side legs of the given stirrup. For most of the test, Stirrup 4 (furthest from the node zone) developed the highest tensile strain. Stirrup 1 (located within the nodal zone and closest to the head) developed a small compressive strain. All stirrups, however, began to develop significant tensile strains near failure. Shortly after the formation of Crack 2 (near a bearing reaction of about 275 kN), Stirrup 1 developed tensile strain. Near failure, Stirrup 1 reached higher tensile strains than the other stirrups. This was most likely a result of the formation of a bearing wedge at the head of the tie bar. This wedge acted to cleave the concrete, causing large vertical tension. Even with a closely spaced stirrup to counteract tension caused by the wedge, capacity was not improved; however, the stirrup helped to produce a more ductile failure than that of companion unconfined specimens. The data from Fig. 14 and 16 are presented in the form of strain

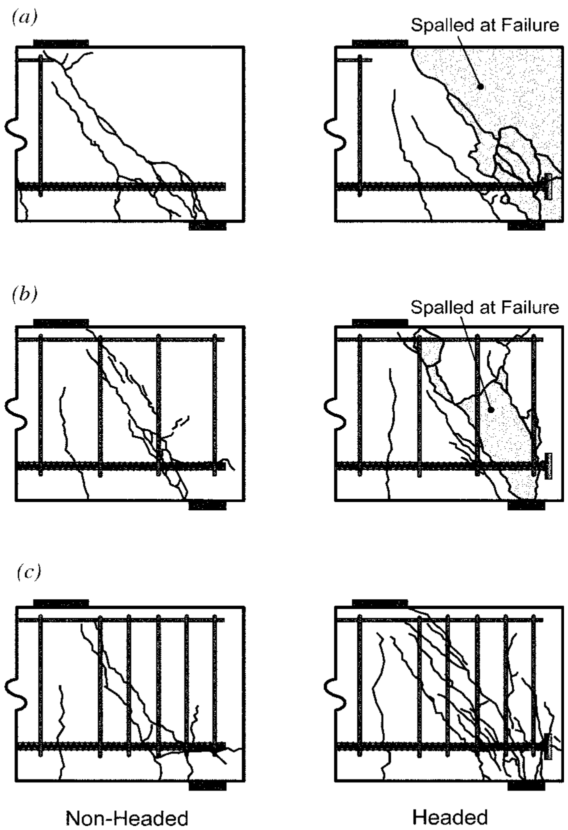

Fig. 18—Crack patterns at failure for CCT nodes anchoring headed and nonheaded reinforcement: (a) no confinement; (b) light confinement (10 mm hoop stirrups at 152 mm); and (c) heavy confinement (10 mm hoop stirrups at 76 mm).

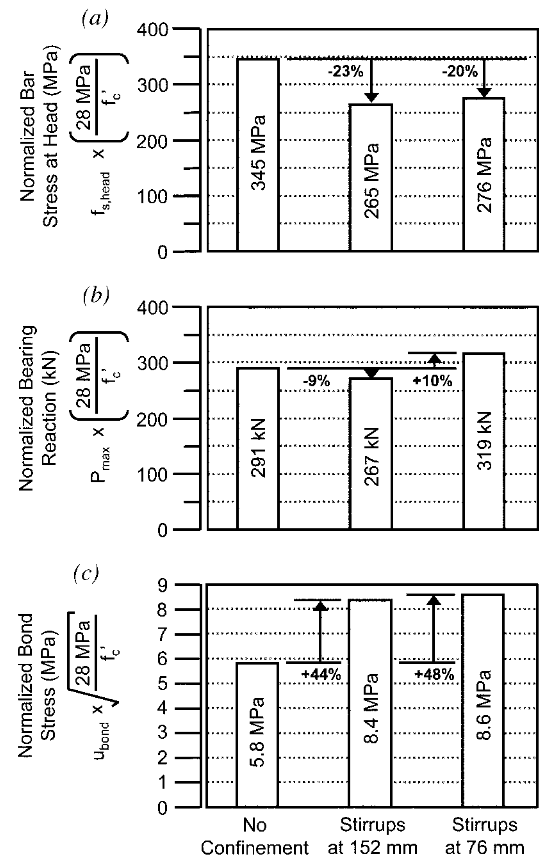

Fig. 19—Capacity of CCT nodes with various amounts of confinement: (a) bar stress at head; (b) bearing reaction at node; and (c) average bond stress at failure.

profiles in Fig. 17. Profiles from a companion nonheaded specimen are presented for comparison.

Crack patterns at failure for nonheaded and headed specimens with various amounts of confinement are shown in Fig. 18. There is little difference between the failures of the three nonheaded specimens. With or without stirrups, failure was governed by bar pullout. Additionally, the final crack pattern was characterized by a wide single crack propagating from the edge of the bearing plate at the CCT node to the edge of the load plate at the top of the diagonal strut.

For specimens with headed tie bars, the final crack pattern was more complex and changed with the inclusion of stirrups. In the unconfined specimen, lateral spalling resulted in a web of cracks near the node. These cracks tapered together into a single diagonal crack that propagated to the top load plate. The concrete above this crack fractured off as a single block. In the heavily confined specimen, diagonal cracking was distributed into a broad band of closely spaced cracks and no spalling occurred. The lightly confined specimen showed transition behavior between the other two. Diagonal cracking was distributed over a larger band than in the unconfined specimen, but not as broadly as in the heavily confined specimen. Some spalling occurred, but not as severe as the unconfined specimen.

The capacities of the confined specimens with headed bars are compared to a companion unconfined specimen in Fig. 19. The data show that bar stress at the head decreased when confinement was added (Fig. 19(a)). It is possible that the confinement hindered concrete placement around the node, resulting in a decrease in head bearing capacity.

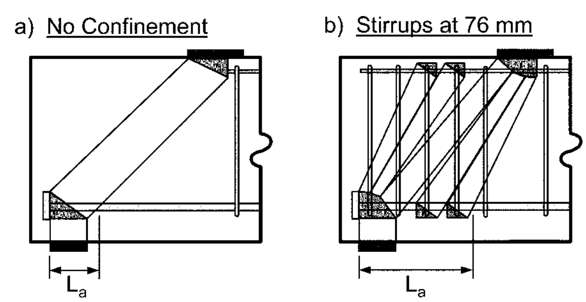

Fig. 20—Truss mechanisms at confined and unconfined CCT nodes.

For the specimen with stirrups at 76 mm, confinement caused a 20% decrease in bar stress at the head; however, there was a 10% increase in the bearing reaction at the node (Fig. 19(b)). The overall increase to capacity is accounted for by bond. The bond contribution was increased for two reasons. First, the stirrup confinement restrained splitting and resulted in an increase in the bond stress along the bar. Average bond stresses at failure were calculated using stress data at two points along the bar (at $1d_b$ and $7d_b$ from the head). The values are plotted in Fig. 19(c). Average bond stress at failure increased by about 48% with the addition of 10 mm hoop stirrups at 76 mm. Secondly, the anchorage length of the tie bar was increased because of changes to the truss mechanism. The addition of stirrups provided an alternate path for diagonal compression struts (refer to Fig. 20). Subsequent fanning of the strut path allowed the anchorage length to increase. In addition to the changes caused to bond stress and the truss mechanism, stirrup confinement also provided improved ductility and a better distribution of cracking.

CONCLUSIONS

Behavior of CCT nodes

Based on the results of this study, the following conclusions can be made:

1. The location of the critical anchorage point (at which maximum tie bar stress is achieved) in a CCT node can be estimated as the intersection of the tie bar with the edge of the diagonal compression strut that is anchored by that tie bar. This is the boundary of the extended nodal zone. Appendix A of the ACI code[5] already recommends the edge of the extended nodal zone as the critical anchorage point. The results of this study verified that recommendation.

2. The state of stress at a CCT node reversed on either side of the critical crack. Beneath the CCT node, compression stresses from the lower bearing plate necked inward to equilibrate spatially with the bearing face of the headed bar. This created a region of biaxial compression that began at the bearing face of the head and continued to the edge of the extended nodal zone. Beyond the extended nodal zone, radial splitting stresses created by bond of the reinforcing bar caused a state of tension within the concrete.

3. CCT nodes fail by mechanisms related to anchorage. Nonheaded bars failed by pullout from the node. Headed bars failed by explosive rupture at the node. Rupture was characterized by crushing just above the head and lateral splitting of the diagonal strut. The extent to which these two characteristics governed behavior depended on head size and orientation.

4. Variations in strut angle affect the anchorage length of the tie bar. Shallow strut angles increased the length of the extended nodal zone, moving the critical development point away from the head and increasing the contribution from bond to anchorage.

5. Stirrup confinement increased the anchorage length of the tie bar by changing the truss mechanism. Additionally, bond stress, ductility, and crack control were improved by the addition of stirrups.

Anchorage behavior of headed bars

6. The anchorage of headed bars was mobilized in two stages. In the first stage, anchorage was carried almost entirely by bond stress, which peaked as the first stage ended. In the second stage, as bond began to deteriorate, bar stress was transferred to the head. Throughout the second stage, bond declined and head bearing increased. The second stage ended with yielding of the bar or bearing failure of the concrete at the head. As a result of this behavior, peak bond and peak head bearing did not occur simultaneously. The capacity of the bar at failure was determined by the peak bearing capacity plus some contribution from reduced bond along the bar between the head and the point of peak bar stress.

7. Bond stress at failure decreases as relative head area increases. The larger the relative head area, the longer the interval over which bar stress was transferred to the head and bond stress declined. Thus, larger head size was accompanied by lower bond at failure.

8. Slip of the head decreased as head size was increased. Slip occurred in two stages: insignificant head slip occurred before the head attained most of its capacity. Shortly before peak bearing capacity was reached, slip increased steadily until failure occurred.

ACKNOWLEDGMENTS

The support of the Texas Department of Transportation and the guidance of the project supervisor D. Van Landuyt is gratefully acknowledged. The test program was conducted at the Ferguson Structural Engineering Laboratory of the University of Texas at Austin. The help of the laboratory staff and special efforts of graduate students M. Ziehl and A. Ledesma were essential to the conduct of the study.

NOTATION

A_b	=	bar area, mm^2
A_{gh}	=	gross head area, mm^2
A_{nh}	=	net head area, $A_{gh} - A_b$, mm^2
A_{sv}	=	area of stirrup reinforcement, mm^2
b	=	specimen width or strut width, mm
d_b	=	bar diameter, mm
f'_c	=	concrete compression strength, from cylinder tests, MPa
$f_{s,head}$	=	bar stress at head, MPa
P	=	bearing reaction at CCT node, kN
s	=	spacing of stirrup reinforcement, mm
u_{bond}	=	average bond stress, MPa
δ_h	=	head slip, mm
θ_{strut}	=	strut angle, measured between axis of tie bar and axis of strut

REFERENCES

1. Barton, D. L.; Anderson, R. B.; Bouadi, A.; Jirsa, J. O.; and Breen, J. E., "An Investigation of Strut-and-Tie Models for Dapped Beam Details," *Center for Transportation Research Report* No. CTR 3-5-87/9-1127-1, Austin, Tex., May 1991.

2. Armstrong, S. D.; Salas, R. M.; Wood, B. A.; Breen, J. E.; and Kreger, M. E., "Behavior and Design of Large Structural Concrete Bridge Pier Overhangs," *Center for Transportation Research Report* No. CTR-1364-1, Austin, Tex., Feb. 1997.

3. Wood, B. A.; Kreger, M. E.; and Breen, J. E., "Experimental Investigation of Design Methods for Large Cantilever Bridge Bents," *Center for Transportation Research Report* No. CTR-1364-3F, Austin, Tex., Aug. 1997.

4. Aguilar, G.; Matamoros, A.; Parra-Montesinos, G.; Ramirez, J. A.; and Wight, J. K., "Experimental and Analytical Evaluation of Design Procedures for Shear Strength of Deep Reinforced Concrete Beams," *Final Report to the Reinforced Concrete Research Council*, Purdue University, West Lafayette, Ind., May 2001.

5. ACI Committee 318, "Building Code Requirements for Structural Concrete (ACI 318-02) and Commentary (318R-02)," American Concrete Institute, Farmington Hills, Mich., 2002, 443 pp.

6. Thompson, M. K.; Jirsa, J. O.; Breen, J. E.; and Klingner, R. E., "Anchorage Behavior of Headed Reinforcement: Literature Review," *Center for Transportation Research Report* No. 1855-1, Austin, Tex., May 2002.

7. Thompson, M. K.; Young, M. J.; Jirsa, J. O.; Breen, J. E.; and Klingner, R. E., "Anchorage of Headed Reinforcement in CCT Nodes," *Center for Transportation Research Report* No. 1855-2, Austin, Tex., May 2002.

8. Thompson, M. K.; Ledesma, A. L.; Jirsa, J. O.; Breen, J. E.; and Klingner, R. E., "Anchorage Behavior of Headed Reinforcement," *Center for Transportation Research Report* No. 1855-3, Austin, Tex., May 2002.